Earth and Planetary Science Letters 278 (2009) 152–162

Contents lists available at ScienceDirect

Earth and Planetary Science Letters

journal homepage: www.elsevier.com/locate/epsl

Synthetic tomography of plume clusters and thermochemical piles

A.L. Bull [a,*], A.K. McNamara [a], J. Ritsema [b]

[a] School of Earth and Space Exploration, Arizona State University, Tempe, AZ, 85287-1404, United States
[b] Department of Geological Sciences, University of Michigan, Ann Arbor, MI, 48109, United States

ARTICLE INFO

Article history:
Received 15 May 2008
Received in revised form 3 November 2008
Accepted 16 November 2008
Available online 22 January 2009

Editor: C.P. Jaupart

Keywords:
mantle convection
isochemical
plume clusters
thermochemical piles
tomography

ABSTRACT

Seismic tomography elucidates broad, low shear-wave velocity structures in the lower mantle beneath Africa and the central Pacific with uncertain physical and compositional origins. One hypothesis suggests that these anomalies are caused by relatively hot and intrinsically dense material that has been swept into large thermochemical piles by mantle flow. An alternative hypothesis suggests that they are instead poorly imaged clusters of narrow thermal plumes. Geodynamical calculations predict fundamentally different characters of the temperature fields of plume clusters and thermochemical piles. However the heterogeneous resolution of tomographic models makes direct comparison between geodynamical temperature fields and tomographic shear-wave anomalies tenuous at best. Here, we compute synthetic tomographic images for 3D spherical mantle convection models and evaluate how well thermal plumes and thermochemical piles can be reconciled with actual seismic tomography images. Geodynamical temperature fields are converted to shear-wave velocity using experimental and theoretical mineral physics constraints. The resultant shear-wave velocity fields are subsequently convolved with the resolution operator from seismic model S20RTS to mimic the damping and distortion associated with heterogeneous seismic sampling of the mantle. We demonstrate that plume clusters are tomographically blurred into two broad, antipodal velocity anomalies in agreement with S20RTS and other global seismic models. Large, thermochemical piles are weakly distorted by the tomographic filter. The power spectrum of velocity heterogeneity peaks at spherical harmonic degree 3, unlike the degree-2 maximum in S20RTS, but decays rapidly similar to S20RTS and many other seismic models. Predicted tomography from thermochemical pile and plume cluster models correlate equally well with S20RTS given the uncertainties in the numerical modeling parameters. However, thermochemical piles match tomography better in visual comparison and in the overall character of the harmonic spectrum.

1. Introduction

Understanding the nature of large-scale mantle convection remains a critical goal in solid-Earth geophysics. A fundamental question rests on whether the driving forces causing mantle convection are primarily thermal (i.e., isochemical convection) or both thermal and compositional (i.e., thermochemical convection). It is important to distinguish between these given that each has unique consequences for the mode of heat and mass transport within the Earth's interior.

Seismic tomography provides a constraint on the present state of wave speed heterogeneity in the Earth's mantle. Combined with hypothesis-testing through geodynamical modeling and an understanding of the mineral physics, it can provide a useful constraint toward developing a conceptual model of mantle convection.

Recent tomographic observations (Fig. 1a and b) reveal a lower mantle characterized by higher-than-average shear-wave speeds beneath Asia and encircling the Pacific which are consistent with cold slabs of descending lithosphere beneath regions of ancient subduction (e.g., Ricard et al., 1993; van der Hilst et al., 1994; Grand et al., 1997; Bunge et al., 1998; Lithgow-Bertelloni and Richards, 1998), and lower-than-average shear-wave speeds in broad regional areas beneath Africa and the central Pacific (e.g., Dziewonski et al., 1977; Grand, 1994; Su et al., 1994; Masters et al., 1996, Ritsema et al., 1999, 2004; Mégnin and Romanowicz, 2000). The large, negative shear-wave velocity anomalies, although not as easily understood from a dynamical perspective, are inferred to be characterized by broad upwelling centers between Mesozoic and Cenozoic subduction zones.

Geodynamical studies of whole-mantle, isochemical convection using typical material parameters reveal a correlation between predicted cold downwellings and observed faster-than-average shear wavespeeds (Bunge et al., 1998; McNamara and Zhong, 2005; Richards et al., 2000), but do not predict the presence of large megaplumes on the same scale as the observed low shear-wave velocity anomalies. Instead, predicting smaller thermal plumes which cluster beneath Africa and the Central Pacific (Fig. 2a, b) (e.g., Bunge et al., 1998; Zhong et al., 2000; Schubert et al., 2004; McNamara and Zhong, 2005). Furthermore, Grigné et al. (2007) and Guillou and Jaupart (1995)

* Corresponding author. Tel.: +1 480 727 9121; fax: +1 480 965 8102.
E-mail address: abigail.bull@asu.edu (A.L. Bull).

0012-821X/$ – see front matter © 2008 Elsevier B.V. All rights reserved.
doi:10.1016/j.epsl.2008.11.018

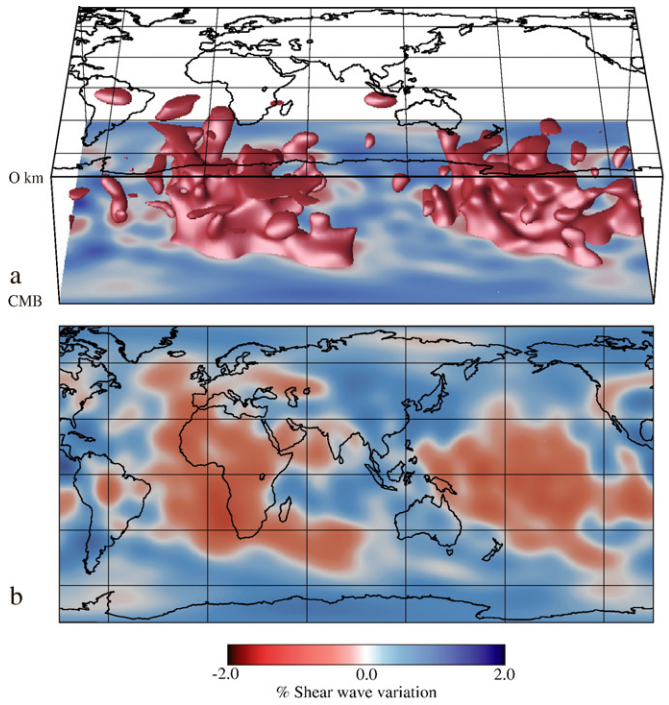

Fig. 1. Shear-wave velocity heterogeneity for the tomographic model S20RTS (Ritsema et al., 1999, 2004) shown (a) as an isosurface in cross-sectional view through the mantle and (b) in map view at 2750 km depth. Both views reveal a lower mantle dominated by the large low shear-wave velocity anomalies beneath Africa and the Pacific. Present-day tectonic plate boundaries are superimposed on each plot.

showed that sets of small thermal plumes collect beneath continent-like heterogeneities for high Rayleigh numbers while Nolet et al. (2006) and Boschi et al. (2007, 2008) have quantitatively compared dynamic models of plumes with seismic tomography observations. Montelli et al. (2004) used finite-frequency tomography to study the existence and character of deep-mantle thermal plumes.

Geodynamical studies of mantle models involving a thermochemical component (e.g., Tackley, 1998, 2002; Davaille, 1999; Kellogg et al., 1999; Ni et al., 2002; Jellinek and Manga, 2004; McNamara and Zhong, 2004, 2005; Davaille et al., 2005; Tan and Gurnis, 2005, 2007; Simmons et al., 2007), such as thermochemical piles (e.g., Tackley, 1998, 2002; Jellinek and Manga, 2004; McNamara and Zhong, 2004, 2005), metastable superplumes (e.g., Tan and Gurnis, 2005) and thermochemical superplumes (e.g., Davaille, 1999) result in high temperature anomalies that resemble the large negative shear wave velocity anomalies observed in seismic tomography (McNamara and Zhong, 2005). These models are further supported by geochemical observations of multiple chemical reservoirs at depth (e.g., Hofmann, 1997), strong seismic contrasts (e.g., Breger and Romanowicz, 1998; Ritsema et al., 1998; Ni et al., 2002; Wang and Wen, 2004; Ford et al., 2006) and increased density in these regions (Ishii and Tromp, 1999; Deschamps and Trampert, 2003; Deschamps et al., 2007; Hernlund and Houser, 2008). The various thermochemical models differ in their dynamical behavior but all involve similar large volumes of intrinsically dense material within broad upwelling regions and all relate the African and Pacific anomalies to large structures of intrinsically more-dense composition. In this study, we concentrate on the conceptual model of "thermochemical piles" (e.g., Tackley, 1998, 2002; Jellinek and Manga, 2004; McNamara and Zhong, 2004, 2005), whereby a dense basal layer has been pushed aside by lower mantle downwellings and has accumulated in ridge-like structures in the African and Pacific upwelling regions (Fig. 2c, d).

Typically, temperature fields from geodynamical results are directly compared to tomographic models (e.g., Becker and Boschi, 2002; Davaille et al., 2005; McNamara and Zhong, 2005) to investigate the first order dynamics and compositional structure of Earth's mantle. However, this simple comparison is fraught with uncertainty: for one, the resolution of geodynamical models is typically much higher than that of tomographic models and the combined effect of both chemistry and temperature on seismic wavespeeds is difficult to assess from simply comparing temperature and compositional fields to tomography. Furthermore, numerical models employ a relatively regular mesh providing uniform resolution which contrasts with the heterogeneous coverage obtained by seismic tomography due to an incomplete and uneven distribution of earthquakes and seismic stations. Direct compariSson between geodynamical temperature fields and tomographic models also assumes purely temperature dependence of seismic velocity, ignoring the pressure- and compositional dependence. Consequently, tomographic models distort thermal and chemical heterogeneity, resulting in a blurred image of mantle structure. Indeed, recently, Schubert et al. (2004) proposed that large contiguous structures beneath Africa and the Pacific may not be required to create the observed lower mantle shear-wave velocity structure. They suggested that limited tomographic resolution is responsible for poorly imaged clusters of isochemical thermal plumes. At first glance, this explanation does not reconcile the geochemical and seismic evidence for compositional heterogeneity. However, this isochemical conceptual model may be extended to include chemical heterogeneity as long as the intrinsically dense material is of small volume or if its density contrast with the surrounding mantle is small. In either case, clusters of small thermal plumes are still expected to form in the presence of chemical heterogeneity (Garnero and McNamara, 2008). Therefore, in this paper we refer to an isochemical model as a model that produces clusters of plumes, whether compositional heterogeneity is actually associated with it or not.

A more appropriate comparison is to use experimental and theoretical mineral physics relationships to convert geodynamical temperature and composition fields to seismic velocity as a function of temperature, pressure, and composition. The resultant velocity anomaly fields are then filtered to capture the inherent heterogeneous resolution associated with a particular tomographic model. This leads to the creation of "synthetic" tomographic models and allows for a more meaningful comparison between geodynamic and seismic models.

In this study, we combine 3D spherical geodynamic and mineral physics calculations to create synthetic seismic tomography from geodynamical calculations of two hypothetical large-scale mantle models. The first is dynamically isochemical in which clusters of thermal plumes form in the lower mantle beneath Africa and the central Pacific. The second is a thermochemical model, in which a uniform 255 km thick intrinsically dense basal layer is perturbed by large scale convective flow. We convert the resultant geodynamical temperature and composition fields to seismic velocity, and apply a "tomographic-filter" (e.g., Mégnin et al., 1997; Bunge and Davies, 2001; Ritsema et al., 2007) to produce synthetic tomography models which we compare to the global shear-wave tomography model S20RTS (Ritsema et al., 1999, 2004), both visually and statistically, to determine whether the geodynamic models match the seismic observations.

The fundamental motivation is to determine whether, if we take into account the heterogeneous nature of tomographic resolution, observations of seismic tomography can be used as a constraint to distinguish between these competing conceptual mantle models as a possible cause of the observed lower mantle seismic anomalies beneath Africa and the central Pacific. We find the tomographic filtering has a significant effect, particularly on the plume cluster models. We determine that the seismic filter considerably broadens and distorts the theoretical images of plume clusters. The images of thermochemical piles are less distorted unless the piles are composed of material that has a higher intrinsic shear-wave velocity than the surrounding mantle. Synthetic tomography from thermochemical models matches the S20RTS maps and spectrum slightly better than

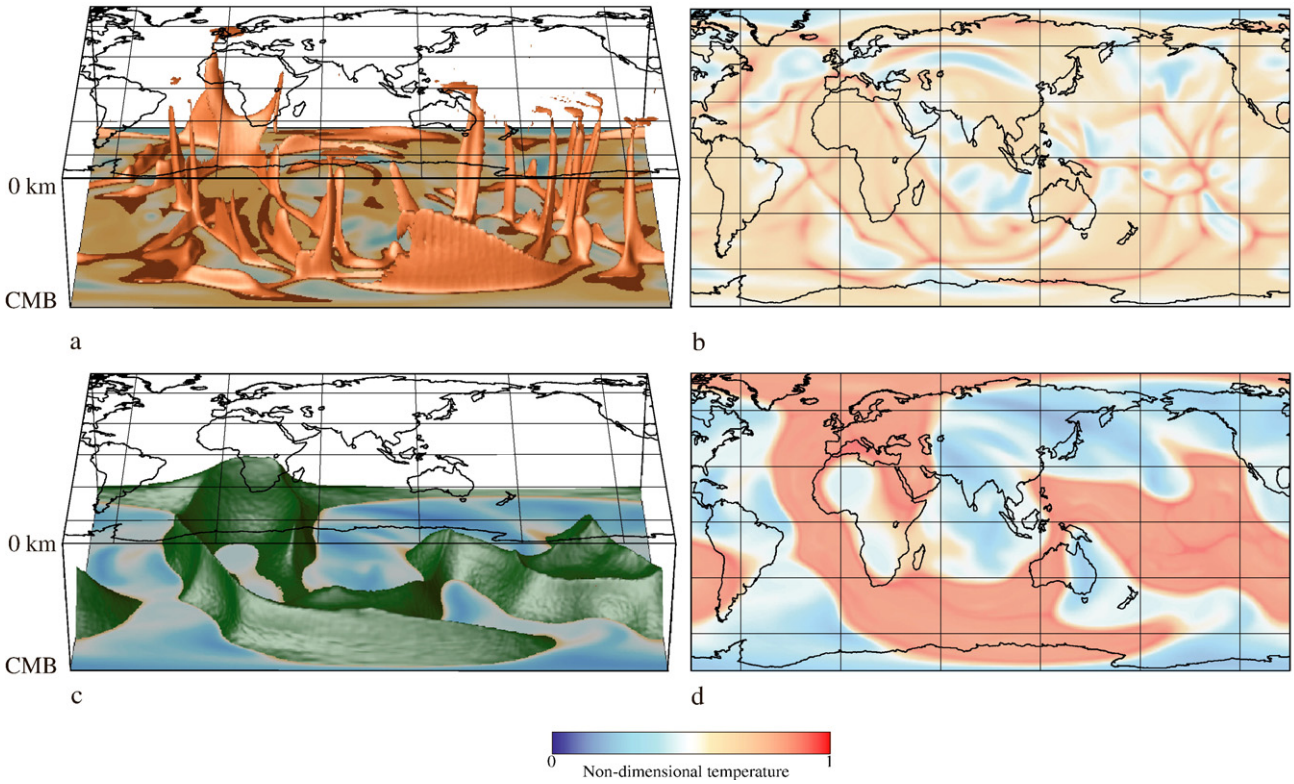

Fig. 2. Geodynamic calculation results. (a) A temperature isosurface in cross-sectional view through the mantle and (b) lowermost mantle temperature map for the plume cluster model reveal small-scale upwellings that are focused into clusters of plumes beneath Africa and the Pacific. (c) Compositional isosurface in cross-sectional view through the mantle and (d) lowermost mantle temperature map for the thermochemical pile model show a large ridge-like structure beneath Africa and a superposition of ridges beneath the Pacific. Present-day tectonic plate boundaries are superimposed on each plot. Map views are at 2750 km depth.

does the isochemical model. However, given the uncertainty in geodynamical modeling parameters, a straightforward analysis indicates that the improved match is statistically insignificant.

1.1. Previous Work

McNamara and Zhong (2005) performed 3D spherical geodynamical calculations of thermochemical piles and isochemical plume clusters using the thermochemical extension of the 3D finite-element convection code CitcomS (e.g., Zhong et al., 2000; McNamara and Zhong, 2004). The modeling procedure is detailed in Appendix A.

The models employed a Rayleigh number of 2.7×10^8, featured internal and bottom heating (non-dimensional heat production of 10) and temperature- and depth-dependent rheology in a spherical Earth which led to a weak upper mantle, a 30× viscosity step at the upper–lower mantle boundary, and a 10× linear increase with depth to the base of the mantle. Both calculations started with one-dimensional geotherms from similar calculations which had reached temperature equilibrium and are identical but for one exception: the thermochemical pile model initially incorporated an intrinsically dense (~3% denser than the ambient mantle) layer in the lowermost 255 km of the mantle. In order to guide the location of subduction, plate motions for the past 119 million years were imposed as surface boundary conditions (e.g., Bunge et al., 1998; Lithgow-Bertelloni and Richards, 1998). The Rayleigh number was carefully chosen such to minimize artificial forcing of the kinematic boundary conditions onto the convective system to an insignificant level.

Geodynamical model results from the calculations of McNamara and Zhong (2005), projected onto a Cartesian box, are shown in Fig. 2. In the isochemical model (Fig. 2a and b), clusters of thermal plumes form in the central Pacific and along a N–W trending upwelling region beneath Africa. For the thermochemical model (Fig. 2c and d), large-scale convection sweeps the basal layer into a large, ridge-like structure beneath Africa and into several overlapping ridges beneath the Pacific, similar to observations in other studies (e.g., Tackley, 1998, 2002; Jellinek and Manga, 2002, 2004).

Direct comparison of the temperature maps of the isochemical "plume cluster" model (Fig. 2b) and the thermochemical "pile" model (Fig. 2d) to the observed shear-wave velocity structure in S20RTS (Fig. 1b) suggested that the thermochemical model better reproduced the broad low shear-wave anomalies seen in the tomographic model: the anomalies in the plume cluster model were too small scale.

In Ritsema et al. (2007), the authors took a straightforward and classical approach to introducing tomographic artifacts into the geodynamic models of McNamara and Zhong (2005). The fundamental motivation was to determine how artifacts distort tomographic images and complicate model interpretation, and the authors investigated thermochemical and isochemical end member models of mantle convection. A simple, linear relationship between temperature and shear-wave velocity was employed, a homogeneous composition for both models was assumed, and pressure-dependence was excluded. Seismic velocity fields determined for the isochemical and thermochemical geodynamic models were projected into the spatial parameterization of the global shear-wave tomographic model S20RTS (Ritsema et al., 1999, 2004) and subsequently convolved with the tomographic model's resolution operator (e.g., Menke, 1989; Bunge and Davies, 2001). This work demonstrated that short-wavelength structure and strong velocity gradients are suppressed in tomographic images and seismic structures may be artificially stretched and tilted.

In the current study, we extend these previous efforts to include appropriate physical relationships between seismic velocity and temperature, pressure, and composition. We investigate scenarios in which the thermochemical material has a higher intrinsic shear-wave velocity than surrounding mantle material, and we examine how

different assumptions of core–mantle boundary (CMB) temperature affect the results.

2. Method

We use the temperature and composition fields from the isochemical and thermochemical geodynamic models of McNamara and Zhong (2005) described in Section 1.1 (Fig. 2). The geodynamical calculations produce non-dimensional temperature fields which we convert to dimensional temperatures. This conversion depends on the mantle adiabat which must be added to the potential temperatures obtained in the Boussinesq calculations. This isentropic temperature gradient is proportional to the temperature and is defined as

$$\left(\frac{dT}{dz}\right)_s = \frac{\alpha_v g T}{C_p}$$

where α is the coefficient of thermal expansion, g is the gravitational acceleration, T is the temperature and C_p is the specific heat at constant pressure. Values for the adiabatic gradient are taken from the results of the thermodynamic code of Stixrude and Lithgow-Bertelloni (2005).

The dimensionalisation of the geodynamic temperature fields is also dependent on the temperature difference between the surface and the core–mantle boundary (CMB). Estimates of CMB temperature vary greatly. For the purpose of this work, we are interested in the overall effect of varying the CMB temperature on our models, and as such we investigate a range of temperatures from 3000 K to 5000 K. This wide range of temperatures may be larger than realistic, however it allows a thorough investigation into the sensitivity of our results to this parameter. We impose a surface temperature of 273 K and investigate three CMB temperatures: 3000 K (consistent with previous studies of this nature, e.g., Kellogg et al., 1999), 3950 K (consistent with recent results on the double-crossing of Post-Perovskite, e.g., Hernlund et al., 2005; van der Hilst et al., 2007) (Alfè et al., 2002), and 4800 K (Knittle and Jeanloz, 1991). The 3950 K temperature is the "reference" temperature which we use for the majority of cases.

We convert the dimensionalized geodynamical temperature fields to pressure- and temperature-dependent shear-wave velocities using the thermodynamic code of Stixrude and Lithgow-Bertelloni (2005), under the assumption that the mantle has a pyrolitic composition (Workman and Hart, 2005) (Fig. 3). This formulation leads to instability of upper mantle minerals at temperatures above 2700 K, so we extrapolate wavespeeds using quadratic polynomials above that temperature in the upper mantle only. However, the pressure–temperature space of the geodynamical models rarely enters this extrapolated regime.

If they exist, the composition of thermochemical piles is unknown. Current hypotheses include reaction products between mantle and core producing Fe-rich silicate sediments (e.g., Buffett et al., 2000; Mao et al., 2006), primordial material (e.g., Kellogg et al., 1999), the segregation of subducted oceanic basaltic crust (e.g., Christensen and Hofmann, 1994; Hirose et al., 2005) and the crystallization of a magma ocean at the base of the mantle (Labrosse et al., 2007). Each of these scenarios implies a different mineralogical composition, most notably an increase in the amounts of either Fe or Si. It has been shown that the main effect of increasing the amount of Fe is dramatically increased densities (Mao et al., 2005) leading to wavespeed reductions. Contrarily, increasing the amount of Si leads to a layer, which, although thermally very hot, is seismically faster than the background material at the same pressure and temperature (e.g., Kellogg et al., 1999). Furthermore, thermochemical convection naturally leads to a considerable amount of entrainment between materials (e.g., McNamara and Zhong, 2004), and as a result, the composition of the pile material will change with time, even if its original source is understood.

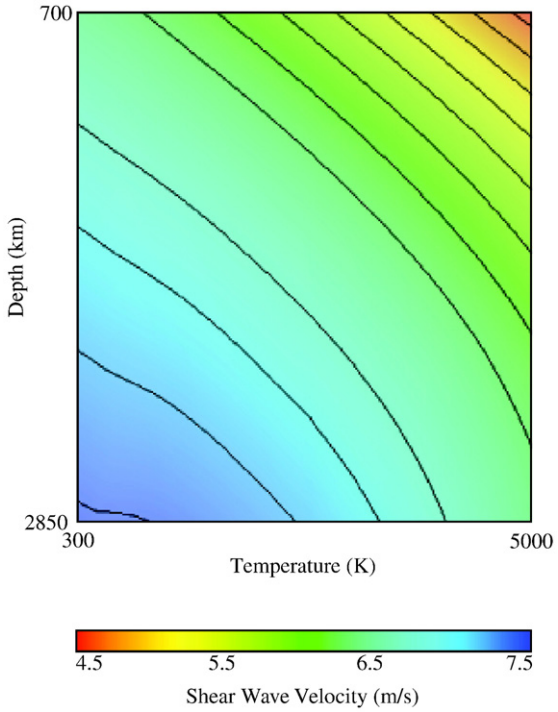

Fig. 3. Contour plot of shear-wave velocity for a bulk mantle composition of Pyrolite as a function of pressure and temperature for the lower mantle (Stixrude and Lithgow-Bertelloni, 2005).

Because of its uncertain origin and the effects of entrainment, we consider it impractical and perhaps misleading for this study to make specific assumptions about the present-day composition of the pile material. Instead, we use an *ad hoc* formulation that assumes the shear-wave velocity of the pile material has the same functional form as pyrolite (i.e., the temperature and pressure derivatives are identical); however, its magnitude is assigned a value that is certain percentage higher or lower than pyrolite, as would result from an enrichment in Si and Fe respectively. We define our formulation:

$$V_{S(pile\ material)}(P,T) = (1+M)V_{S(\mathrm{pyrolite})}(P,T)$$

Where V_S is shear-wave velocity, P is pressure, T is temperature, and M is a constant that we assign. For this study, we investigated a large suite of M values ranging from −0.05 to 0.05 and choose to show values of −0.02, 0.0, 0.03, and 0.04 which are referred to as −2%, 0%, 3%, and 4% in the remainder of the text.

Once shear-wave velocity fields have been generated from the geodynamical temperature and compositional fields, it is imperative that we take into account the heterogeneous nature of tomographic resolution and the subsequent possibility that seismic models may not give a true representation of the lower mantle structure. To do this, we project the predicted seismic velocity fields into the same spatial parameterization as the tomographic model S20RTS (Ritsema et al., 1999, 2004) and convolve them with the tomographic model's resolution operator as described in detail in Ritsema et al. (2007).

We determine the spherical harmonic power spectrum for pre-filtered and post-filtered wave speed fields at each depth level over the lowermost 1000 km of the mantle for each calculation and compare this to tomography by calculating the misfit Q defined as:

$$Q = \sum_{z=1}^{z=z\max} \sum_{l=0}^{l=12} \frac{[G(l)-T(l)]^2}{[T(l)]^2},$$

where z represents a particular depth slice of the calculation, l is the spherical harmonic degree, and $G(l)$ and $T(l)$ are the amplitudes of the

Table 1
Description of the models investigated in this study

Model	Model type	CMB temperature (K)	M (%)	Q (prefiltered)	Q (filtered)
IR	Plume cluster	3950	–	0.045	0.076
T1R	Pile	3950	0	0.297	0.108
T2R	Pile	3950	−2	0.484	0.165
T3R	Pile	3950	3	0.095	0.059
T4R	Pile	3950	4	0.058	0.057
IC	Plume cluster	3000	–	0.066	0.100
T1C	Pile	3000	0	0.406	0.104
T2C	Pile	3000	−2	0.146	0.065
T3C	Pile	3000	3	0.046	0.074
T4C	Pile	3000	4	0.048	0.073
IC	Plume cluster	4800	–	0.035	0.059
T1H	Pile	4800	0	0.048	0.017
T2H	Pile	4800	−2	0.693	0.238
T3H	Pile	4800	3	0.226	0.090
T4H	Pile	4800	4	0.159	0.073

Column one lists the case name, column two describes the type of geodynamical model and column three details the core–mantle boundary temperature used in the dimensionalisation of the geodynamical temperature fields. For the thermochemical pile models, column four describes the wavespeed of the intrinsically more dense material relative to the wavespeed of Pyrolite at the same pressure and temperature (Positive percentages are faster than Pyrolite. Negative percentages are slower). Columns five and six give values of the quality factor, Q, which describes how well the power spectra of each model fit that of S20RTS. High values of Q suggest a poor fit. Low values of Q suggest a better fit. Values are shown for the prefiltered and filtered models for each case.

power spectrum at degree l for the geodynamic model and S20RTS, respectively. For comparison purposes, we find that the lower mantle maps give a better representation of the structure compared with this numerical evaluation. However, we do feel that a quantitative measure is also useful. When considering the values of Q calculated using the above formulism, it is important to note that this misfit takes into account only the spectral characteristics between a model and tomography, and does not effectively replace visual inspection. This will be important when interpreting the values of Q for different models.

3. Results

Table 1 lists the cases studied. The isochemical plume cluster and thermochemical pile cases are indicated by the prefixes “I” and “T” respectively. The final letter of each case refers to the CMB temperature employed, where “R” refers to the reference value of 3950 K, “C” refers to the lower bound CMB temperature of 3000 K, and “H” refers to the upper bound CMB temperature of 4800 K. For each thermochemical case, we show 4 different cases for the shear-wave velocity in the pile.

3.1. Investigating temperature- and pressure dependence

Synthetic tomography maps at 2750 km depth are shown for cases IR and T1R in Fig. 4a and b, respectively. These cases assume that shear-wave velocity variations are solely due to temperature and pressure variations (i.e., $M=0.0$), and have an imposed CMB temperature of 3950 K. The reference velocity profile used for calculating the synthetic velocity anomaly is PREM (Dziewonski and Anderson, 1981).

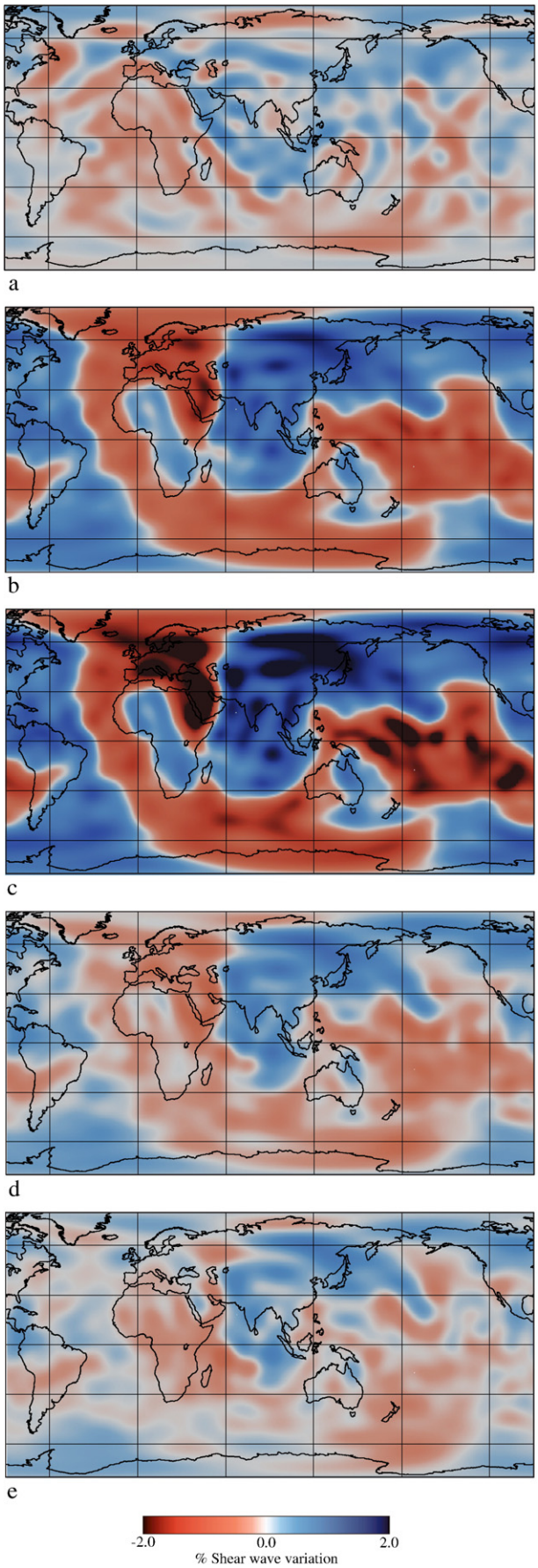

Fig. 4. Predicted lowermost mantle tomographic shear-wave velocity maps for geodynamical models of mantle convection with an imposed core mantle boundary temperature of 3950 K. The color scale is the same as in Fig. 1(a). (a) plume cluster model, (b) thermochemical pile model with no compositional dependence of wavespeed and (c, d, e) thermochemical pile models with wavespeeds −2%, 3% and 4% faster than Pyrolite in the pile material respectively. Present-day tectonic plate boundaries are superimposed on each plot. Map views are at 2750 km depth.

Isochemical case IR shows a low shear-wave velocity anomaly beneath Africa. Comparing it to the original geodynamic temperature field (Fig. 2b), it is obvious that the tomographic filter significantly smoothed the small-scale high temperature anomalies into a contiguous structure which is similar in magnitude to the African anomaly in S20RTS (Fig. 1b). These results suggest that the isochemical model can be reconciled with the large lower mantle anomaly beneath Africa as seen tomographically; however, the cluster of thermal plumes beneath the central Pacific is not projected into a single, large low velocity anomaly. The pre-filtered and post-filtered power spectra of case IR (Fig. 5a) lack the large amplitude, long wavelength component seen in S20RTS. Predicted seismic tomography for thermochemical case T1R shows large contiguous low shear-wave velocity anomalies in the lower mantle beneath Africa and the Pacific. Compared to the original temperature field (Fig. 2d), we note that the tomographic filter has softened the sharp edges of the anomalies (which is most obvious at the northern-most margin of the Pacific anomaly, close to the Aleutians), without changing the anomaly's overall geometry. The thermochemical pile model generates large contiguous anomalies beneath Africa and the central Pacific, albeit that it features a ring-like structure with a seismically fast "hole" beneath central Africa, contrary to seismic observations. The spectrum, shown in Fig. 5b, has a similar redshift as seen in S20RTS but it peaks at degree 3 rather than degree 2.

3.2. Modifying the pile's shear-wave velocity

Synthetic tomographic maps from thermochemical cases T2R, T3R, T4R which examine the effect of changing the shear-wave speed of the pile material (with respect to pyrolite) are shown in Fig. 4c, d and e, respectively. Case T2R (Fig. 4c) shows that a slower shear-wave speed in the pile material results in an increased anomaly magnitude with only minor distortion to the shape of the structures. The synthetic tomography differs little from case T1R. With increasing shear-wave speed in the pile (cases T3R and T4R) the magnitude of shear-wave velocity anomalies is suppressed (Fig. 4d, e). More interestingly, it also blurs the tomographic image of the original structure (compare with Fig. 2d) and fills the hole within the African ring structure. The anomaly is no longer imaged as a ridge-like structure and begins to better resemble the tomography (Fig. 1b), both in shape and velocity anomaly amplitude. The power spectrum of each of these cases is shown in Fig. 5c. Note that as the shear-wave velocity of the pile material increases, the spectral amplitude is reduced, particularly in the lower degrees, and the spectrum flattens out in a manner similar to the isochemical case. Interestingly, case T4R has maximum amplitudes at degree 2 and degree 3.

3.3. Investigating CMB temperature

The dimensional temperatures derived from the geodynamical models are directly proportional to the CMB temperature imposed in our models. Here, we investigate the effect of varying the CMB temperature on our predicted tomography results. We expect variations in the CMB temperature to have a greater effect on the thermochemical models than on the isochemical models, due to the combined effects of composition and temperature in the former.

Cases IC, T1C, T2C, T3C and T4C employ the lower bound temperature of 3000 K. Cases IC and T1C investigate the temperature and pressure dependence of wavespeed, and cases T2C,T3C and T4C investigate the effect of modifying the pile's shear wave velocity. Results for these cases are shown in Fig. 6. In case IC (Fig. 6a), the reduced CMB temperature has acted to suppress the magnitude of the anomalies. The plume clusters are less visible than in case IR but the overall shape of the anomalies is unchanged. In case T1C (Fig. 6b), as with the isochemical model, the imposed lower CMB temperature has acted to suppress the magnitude of the velocity anomalies, however

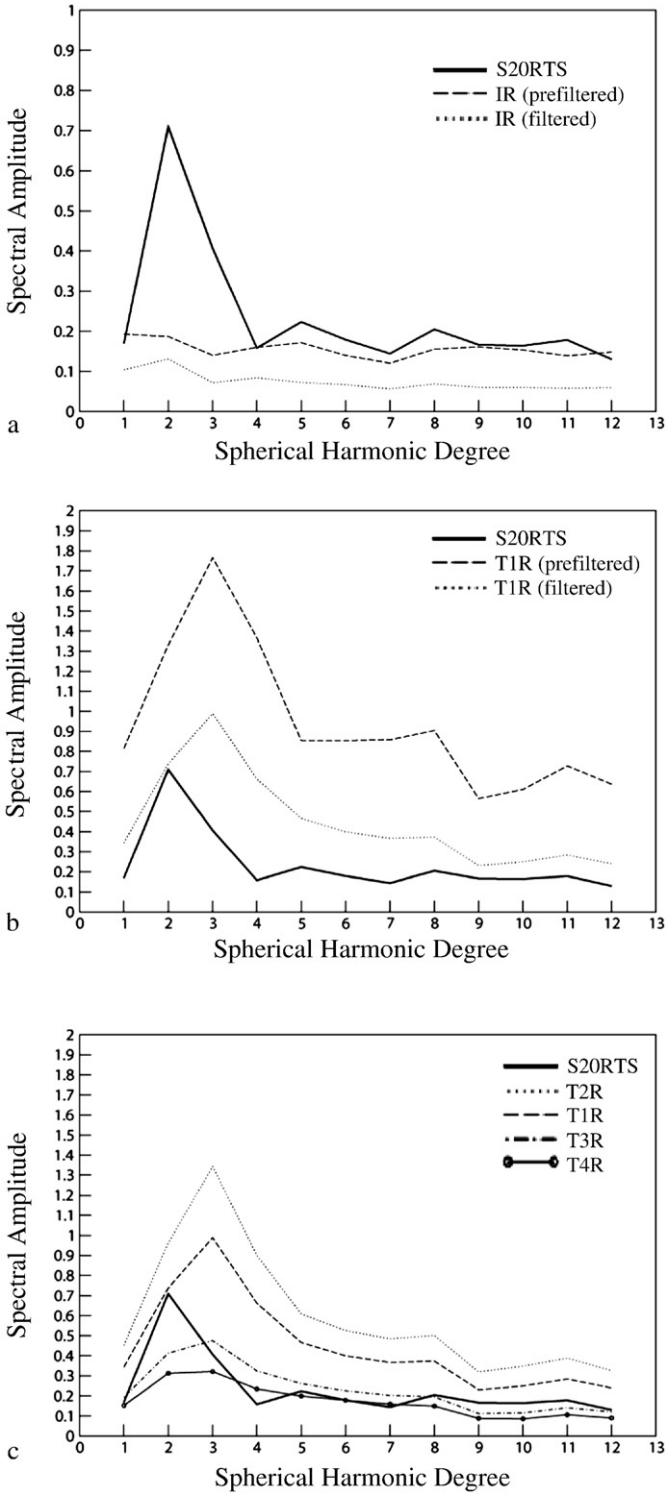

Fig. 5. Spectral amplitude as a function of spherical harmonic degree of shear-wave velocity heterogeneity for (a) IR, (b) T1R, and (c) T2R,T3R and T4R.

there is little noticeable difference between T1R and T1C. In case T2C (Fig. 6c), where the prescribed shear wave velocity in the piles is lower than the ambient mantle, the reduced CMB temperature has little noticeable effect. In cases T3C (Fig. 6d) and T4C (Fig. 6e), the prescribed 3% and 4% increase in shear-wave velocity plays a stronger role than temperature, creating velocity anomalies that are inverted with respect to previous cases. Downwellings have lower shear-wave velocities than the piles, which are now imaged as fast anomalies.

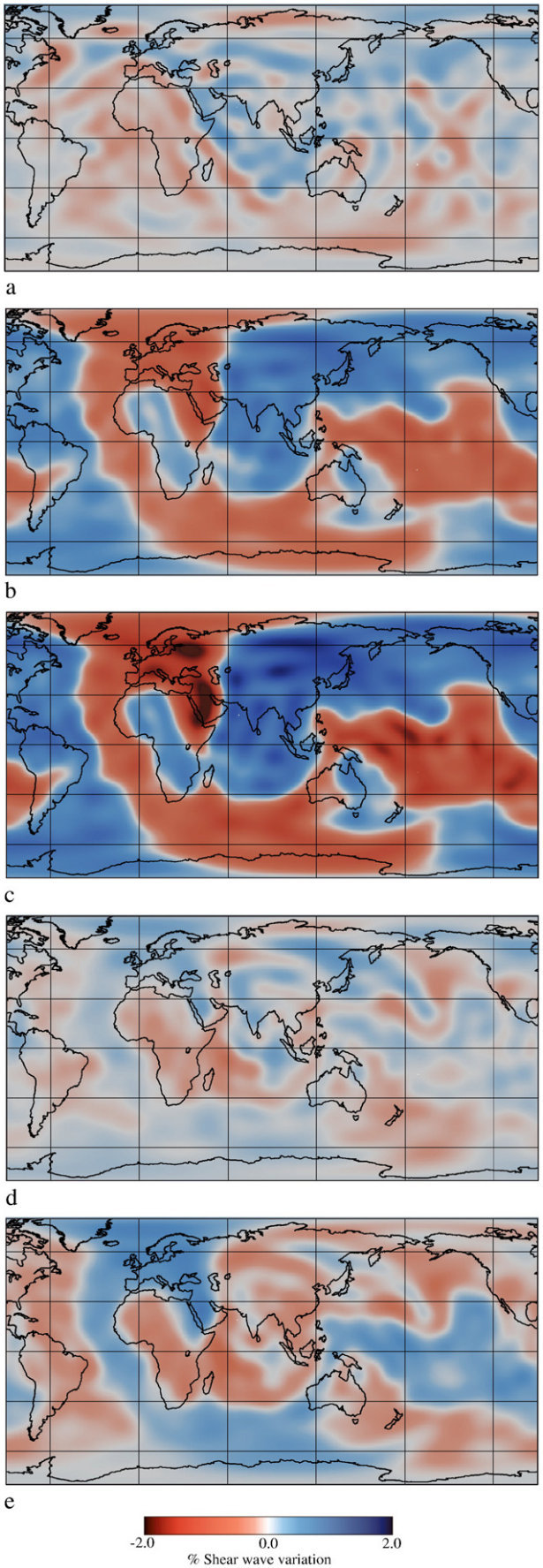

Cases IH, T1H, T2H, T3H and T4H employ the higher CMB temperature of 4800 K. Predicted tomography results for these cases are shown in Fig. 7(a–e respectively). The general shapes of the anomalies remain relatively unchanged, with respect to the reference cases which employ the CMB temperature of 3950 K; however, the velocity anomaly amplitudes are magnified.

The power spectra of the isochemical cases, IC, IR and IH are shown in Fig. 8a. The power spectra of the thermochemical cases, T(1-4)C and T(1-4)H are shown in Fig. 8b and c respectively. We note that increasing the CMB temperature acts to increase the spectral amplitude particularly in the lower degrees, but has no effect on the spectral maxima. All of the thermochemical models peak at degree-3, unlike the degree-2 observed in S20RTS.

4. Discussion

It is important to recognize the uncertainties associated with the modeling aspects of the plume cluster and thermochemical pile hypotheses. While we employ the best estimate of Earth-consistent material properties, many parameters remain relatively unconstrained. These include the rheological formulation (i.e., viscosity), the degree of internal heating, Rayleigh number, and the volume and density of the intrinsically more-dense material in the thermochemical pile models. We have varied the above parameters to confirm that they do not play significant roles in affecting the interpretations of our results. To first order, the spatial characteristics of the piles and plume clusters are not significantly altered. We have varied the Rayleigh number and the viscosity contrast due to temperature dependence by an order of magnitude, the result of which changes the smaller-scale details of pile and plume shape: however the basic geometry of pile material and the overall flow structure remains relatively unchanged. Furthermore, the precise location and orientation of the plume clusters and thermochemical piles are not well constrained due to the uncertainty in the plate motion history and initial conditions, and it is therefore important to consider only the general character of the synthetic tomographic images rather than the detailed morphology of the anomalies.

If thermochemical convection is occurring in Earth's mantle, it is expected to be much richer in complexity than simple models can capture. This work concentrated on one particular thermochemical end member model: primordial, long-lived thermochemical piles. Although continual entrainment of ambient mantle into them is expected to occur, their composition is expected to be relatively homogeneous at any given moment in time. In contrast, if thermochemical piles are composed of segregated oceanic crust that is accumulating in the lower mantle, their internal composition is expected to be more heterogeneous (e.g., Christensen and Hofmann, 1994; Garnero and McNamara, 2008). Thermochemical convection could alternatively take the form of thermochemical superplumes (e.g., Davaille, 1999) or metastable superplumes (e.g., Tan and Gurnis, 2005), each of which would predict a somewhat different geometry of the seismic anomalies. It is therefore important to focus on properties that all of these thermochemical models have in common: intrinsically more-dense material is expected to focus in upwelling regions (i.e., Africa and the Pacific), they will be regional in scale, and they will be significantly hotter than ambient mantle.

Table 1 shows the misfit Q between pre- and post-filtered synthetic tomography and S20RTS. For most cases, the filtered maps match S20RTS maps better than pre-filtered wave speed fields do. The best fitting model is T1H. However, given the uncertainties described in the preceding paragraphs, we consider both isochemical and

Fig. 6. Predicted lower most mantle tomographic shear-wave velocity maps for a) IC (b) T1C (c) T2C (d) T3C and (e) T4C. The color scale is the same as in Fig. 1(a). Present-day tectonic plate boundaries are superimposed on each plot. Map views are at 2750 km depth.

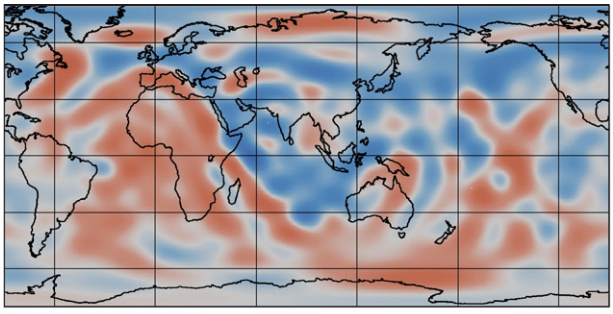
a

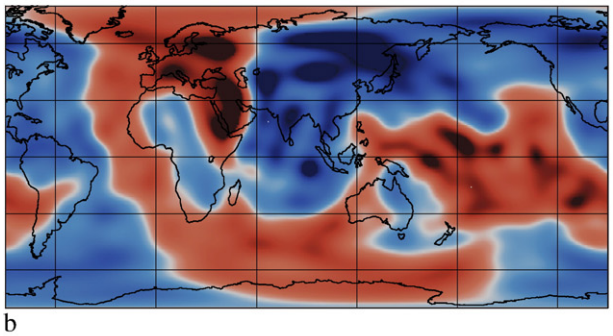
b

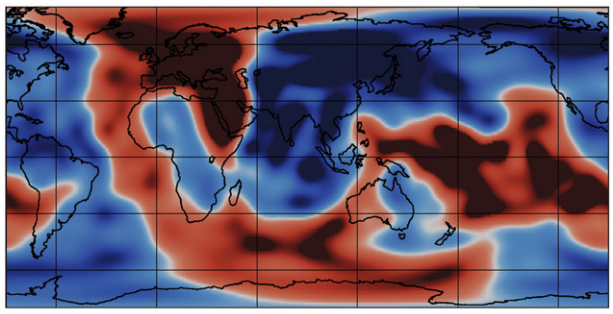
c

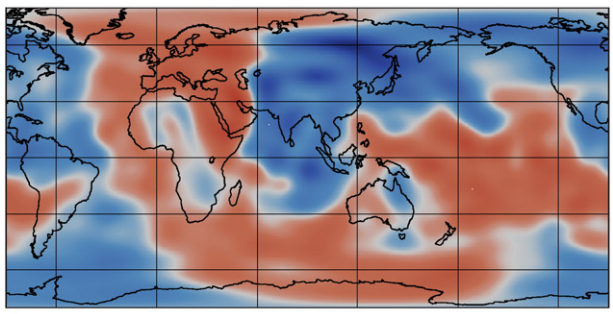
d

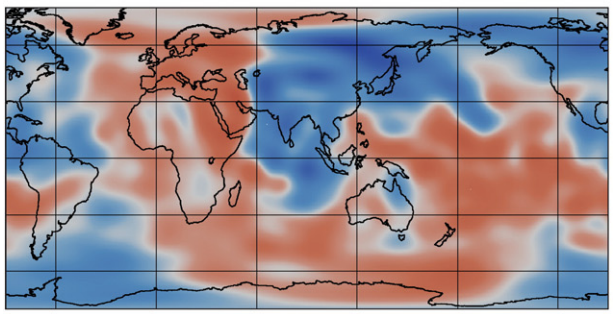
e

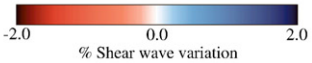

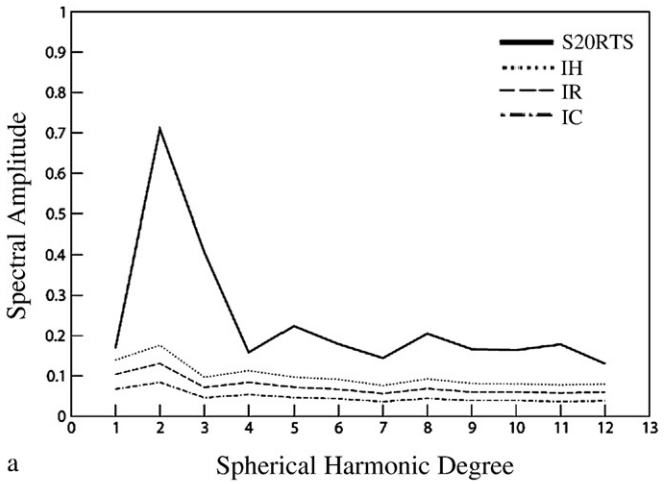

a

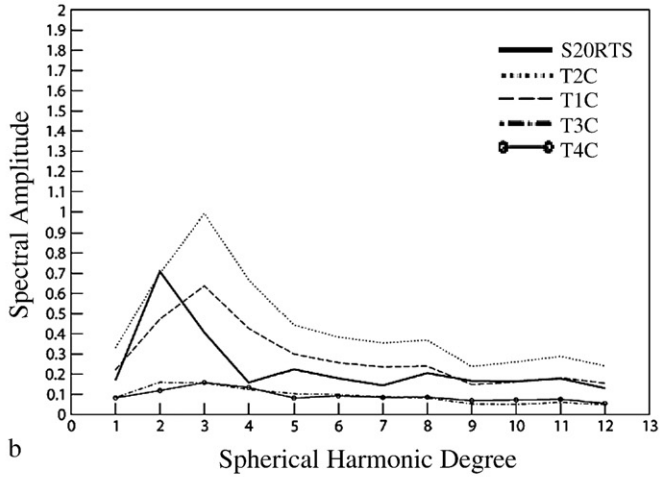

b

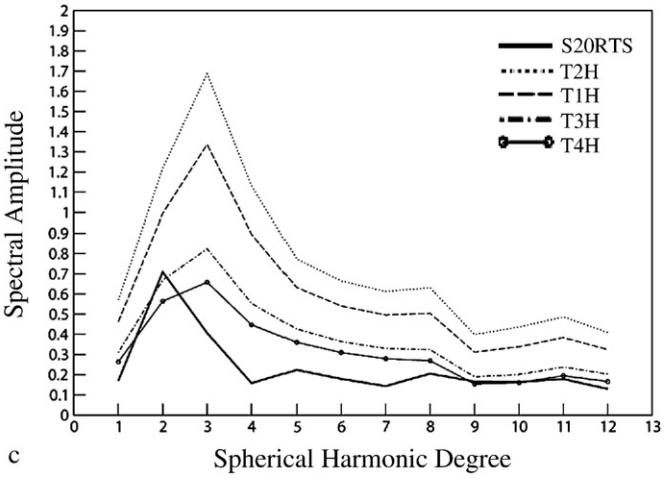

c

Fig. 8. Spectral amplitude as a function of spherical harmonic degree of shear-wave velocity heterogeneity for (a) IC, IR and IH (b) T1-4C, and (c) T1-4H.

thermochemical cases to fit actual tomography equally well, from a statistical standpoint. There are two characteristics that the thermochemical models exhibit that compare better to actual tomography.

Fig. 7. Predicted lower most mantle tomographic shear-wave velocity maps for a) IH (b) T1H (c) T2H (d) T3H and (e) T4H. The color scale is the same as in Fig. 1(a). Present-day tectonic plate boundaries are superimposed on each plot. Map views are at 2750 km depth.

The character of their harmonic spectrum is red-shifted, whereas the plume cluster models have a relatively flattened spectrum. Furthermore, from a more qualitative perspective, the thermochemical models produce more continuous anomalies, similar to that observed in tomography, whereas the plume cluster model predicts a more-spotty anomaly appearance. As stated in the previous section, when considering the values of Q it is important to note that this misfit takes into account both amplitude and character similarities between a model and tomography. This is important when interpreting the value of Q for the isochemical models, which although very dissimilar in amplitude to the power spectrum of tomography, have a character (which can be seen if the power spectra are normalized) very similar to that of S20RTS.

In all thermochemical models, entrainment of ambient mantle is a consistent feature (e.g., Zhong and Hager, 2003; McNamara and Zhong, 2004), the rate of which is very sensitive to density contrast, viscosity, and convective vigor. Throughout thermochemical convection, entrainment leads to a continual exchange and mixing of material from each reservoir. As a result, the intrinsically more-dense material becomes effectively less dense over time and ambient mantle mixes into it. This poses a significant problem for determining the present composition of hypothetical thermochemical structures, even if its source can be assumed or constrained. If thermochemical structures exist, they will have a composition that is an unknown mixture between the original more-dense source material and entrained ambient mantle. Rather than make assumptions regarding this mixture, we used an *ad hoc* formulation that expresses the pile material as being either slower or faster than ambient mantle at the same pressure and temperature conditions. We admit that this formulation is less than ideal, but we maintain that this is the more appropriate approach given realistic uncertainties regarding source and entrainment. Furthermore, we do not account for post-perovskite in this work, which is expected to be present in some regions of the lower-most 200 km of the mantle (e.g., Murakami et al., 2004; Oganov and Ono, 2004; Lay et al., 2006; Ohta et al., 2008).

We find that synthetic tomography images are highly sensitive to CMB temperature. This is an interesting, although not surprising, result with the consequence that regardless how well the mineral physics and mantle composition are understood or how realistic the geodynamical modeling becomes, current CMB temperature constraints are not narrow enough to make unique synthetic tomography images for a given model. It is therefore important that studies investigate several CMB temperatures when predicting seismic tomography from geodynamical models.

This work illustrates that temperature and compositional anomalies in the lower mantle are significantly distorted by the tomographic imaging process, both in terms of anomaly magnitude and shape. Therefore, it is not appropriate to simply compare geodynamic temperature fields to seismic anomalies. This work also highlights the complexity associated with using seismic tomography as a geodynamical constraint. We find that two significantly different geodynamical models (thermochemical and isochemical), each with a distinctly different temperature field, lead to synthetic seismic tomography images that compare relatively equally well to actual tomography from a statistical standpoint, although the thermochemical model better reproduces the long wavelength nature of tomography.

5. Conclusions

This work focused on investigating large-scale mantle structure through mineral-physics based predictions of seismic tomography for two competing conceptual models of mantle convection: thermochemical piles and plume clusters. We investigated the hypothesis that plume clusters could be a possible cause of the observed large, low velocity anomalies in the lower mantle beneath Africa and the Pacific if the heterogeneous nature of tomographic resolution is taken into account. We find the following general conclusions:

1) The tomographic filter distorts and broadens plume clusters. Plume clusters beneath Africa (although not beneath the Pacific) produce anomalies similar to that observed in tomography. Synthetic maps of plume cluster models have maximum spectral amplitude at degree 2, similar to S20RTS and other tomographic models; however, the decay of the power spectrum of velocity heterogeneity is slower than observed.
2) Thermochemical piles are less distorted by the tomographic filter unless they are composed of material with a higher shear modulus than background mantle. Filtered pile models have a spectral maximum at degree 3, unlike the degree 2 maximum observed in seismic models. However, they have a red-shifted spectrum, similar to that observed in seismic models.
3) If thermochemical piles are composed of material with a higher shear modulus than the background material at the same pressure and temperature conditions, their distortion by the filter is more severe, seismic anomalies are smaller, and the spectral fall off is less.
4) The CMB temperature produces the largest uncertainty in the synthetic maps.

Statistically, both isochemical and thermochemical models lead to synthetic seismic tomography images that compare about equally well to actual tomography; therefore, we cannot exclude plume clusters as being a possible cause for the large low shear-wave velocity anomalies observed beneath Africa and the Pacific. However, for the cases studied here, we find that synthetic maps of the thermochemical pile models match S20RTS maps better in terms of reddened spectral character and continuity of anomaly structure.

Acknowledgements

We are indebted to Carolina Lithgow-Bertelloni and Lars Stixrude for making available to us their code and data sets. We thank Amanda Clarke, Matthew Fouch, Ed Garnero and Teresa Lassak for helpful discussions and guidance and four anonymous reviewers for their constructive criticism. This research was supported by NSF grants EAR-0510383 and EAR-0456356.

Appendix A. Geodynamical modeling procedure

The numerical calculations were performed by solving the nondimensional conservation equations of mass, momentum and energy in the Boussinesq approximation. The equation for mass conservation in incompressible flow is

$$\nabla \cdot \mathbf{u} = 0 \tag{1}$$

where $\mathbf{u}$ is the velocity vector. The momentum equation is

$$-\nabla P + \nabla \cdot (\eta \dot{\varepsilon}) = (RaT - RbC)\hat{\mathbf{r}} \tag{2}$$

where $\hat{\mathbf{r}}$ is the radial unit vector, P is the dynamic pressure, η is the viscosity, $\dot{\varepsilon}$ is the strain rate tensor, T is the temperature, C is the composition and Ra is the thermal Raleigh number defined as

$$Ra = \frac{\alpha \rho g \Delta T h^3}{\eta \kappa} \tag{3}$$

where α is the thermal expansivity, ρ is the density, g is the acceleration due to gravity, ΔT is the temperature drop across the mantle, h is the mantle thickness and κ is the thermal diffusivity. We employ a Rayleigh number of 2.7×10^8.

The chemical Rayleigh number, *Rb*, is defined as

$$Rb = \frac{\Delta\rho g h^3}{\eta\kappa} \tag{4}$$

where $\Delta\rho$ is the density contrast between chemical components. A useful non-dimensional quantity is the buoyancy ratio, *B*, which is the ratio of chemical to thermal buoyancy and is defined as

$$B = \frac{Rb}{Ra} = \frac{\Delta\rho}{\rho\alpha\Delta T} \tag{5}$$

The energy equation is defined as

$$\frac{\partial T}{\partial t} + (\mathbf{u}\cdot\nabla)T = \nabla^2 T + H \tag{6}$$

where *t* is time and *H* is the nondimensional internal heating rate. The equation for chemical advection is

$$\frac{\partial C}{\partial t} + (\mathbf{u}\cdot\nabla)C = 0 \tag{7}$$

We employ a temperature- and depth-dependent rheology of the non-dimensional form:

$$\eta(T,\vec{z}) = \eta_r(z)\exp\left[A(0.5-T)\right] \tag{8}$$

where $\eta_r(z)=1$ for $z<663$ km and $\eta_r(z)=0.1225z-51.2$ for 663 km$\leq z\leq$2867 km. η and z are the non-dimensional viscosity and dimensional depth respectively. This formulation leads to a weak upper mantle, a 30× viscosity step at the boundary between the upper and lower mantle, and a 10× linear increase with depth to the base of the mantle. The non-dimensional activation coefficient is chose to be $A=9.2103$, which leads to a temperature-induced viscosity contrast of 10^4. The models are heated from both below and internally with non-dimensional heat production of 10.

References

Alfè, D., Gillan, M.J., Price, G.D., 2002. Composition and temperature of the Earth's core constrained by combining ab initio calculations and seismic data. Earth Planet. Sci. Lett. 195, 91–98.

Becker, T.W., Boschi, L., 2002. A comparison of tomographic and geodynamic mantle models. Geochem. Geophys. Geosys. 3.

Boschi, L., Becker, T.W., Steinberger, B., 2007. Mantle plumes: dynamic models and seismic images. Geochem. Geophys. Geosys. 8 (Q10006). doi:10.1029/2007GC001733.

Boschi, L., Becker, T.W., Steinberger, B., 2008. On the statistical significance of correlations between synthetic mantle plumes and tomographic models. Phys. Earth Planet. Inter. 167, 230–238.

Breger, L., Romanowicz, B., 1998. Three-dimensional structure at the base of the mantle beneath the central Pacific. Science 282, 718–720.

Buffett, B., Garnero, E.J., Jeanloz, R., 2000. Sediments at the top of Earth's core. Science 290, 1338–1342.

Bunge, H.P., Davies, J.H., 2001. Tomographic images of a mantle circulation model. Geophys. Res. Lett. 28, 77–80.

Bunge, H.P., Richards, M.A., Lithgow-Bertelloni, C., Baumgardner, J.R., Grand, S.P., Romanowicz, B.A., 1998. Time-scales and heterogeneous structure in geodynamic Earth models. Science 280, 91–95.

Christensen, U.R., Hofmann, A.W., 1994. Segregation of subducted oceanic crust in the convecting mantle. J. Geophys. Res. 99 (B10), 19,867–19,884.

Davaille, A., 1999. Simultaneous generation of hotspots and superswells by convection in a heterogeneous planetary mantle. Nature 402, 756–760.

Davaille, A., Stutzmann, E., Silveira, G., Besse, J., Courtillot, V., 2005. Convective patterns under the Indo-Atlantic <<box>>. Earth Planet. Sci. Lett. 239, 233–252.

Deschamps, F., Trampert, J., 2003. Mantle tomography and its relation to temperature and composition. Phys. Earth Planet. Inter. 140, 277–291.

Deschamps, F., Trampert, J., Tackley, P.J., 2007. Thermochemical structure of the lower mantle: seismological evidence and consequences for geodynamics. In: Yuen, D., et al. (Ed.), Superplumes: Beyond Plate Tectonics. Springer, Netherlands, pp. 293–320.

Dziewonski, A.M., Anderson, D.L., 1981. Preliminary reference earth model. Phys. Earth Planet. Inter. 25, 297–356.

Dziewonski, A.M., Hager, B.H., O'Connell, R.J., 1977. Large scale heterogeneity in the lower mantle. J. Geophys. Res. 82, 239–255.

Ford, S.R., Garnero, E.J., McNamara, A.K., 2006. A strong lateral shear-wave velocity gradient and anisotropy heterogeneity in the lowermost mantle beneath the southern Pacific. J. Geophys. Res. 111 (B3).

Garnero, E.J., McNamara, A.K., 2008. Structure and dynamics of Earth's lower mantle. Science 320, 626–628.

Grand, S.P., 1994. Mantle shear structure beneath the Americas and surrounding oceans. J. Geophys. Res. 99, 11,591–11,621.

Grand, S.P., van der Hilst, R.D., Widitantoro, S., 1997. Global seismic tomography; a snapshot of convection in the Earth. GSA Today 7, 1–7.

Grigné, C., Labrosse, S., Tackley, P.J., 2007. Convection under a lid of finite conductivity in wide-aspect ratio models: effects of continents on the wave-length of mantle flow. J. Geophys. Res. 112.

Guillou, L., Jaupart, C., 1995. On the effect of continents on mantle convection. J. Geophys. Res. 100, 24217–24238.

Hernlund, J.W., Houser, C., 2008. On the statistical distribution of seismic velocities in Earth's deep mantle. Earth Planet. Sci. Lett. 265, 423–437.

Hernlund, J.W., Thomas, C., Tackley, P.J., 2005. A doubling of the post-perovskite phase boundary and structure of the Earth's lowermost mantle. Nature 434, 882–886.

Hirose, K., Takafuji, N., Sata, N., Ohishi, Y., 2005. Phase transition and density of subducted MORB crust in the lower mantle. Earth Planet. Sci. Lett. 237, 239–251.

Hofmann, A., 1997. Mantle geochemistry: the message from oceanic volcanism. Nature 385, 219–229.

Ishii, M., Tromp, J., 1999. Normal-mode and free-air gravity constraints on lateral variations in velocity and density of Earth's mantle. Science 285, 1231–1236.

Jellinek, A.M., Manga, M., 2002. The influence of a chemical boundary layer on the fixity, spacing and lifetime of mantle plumes. Nature 481, 760–763.

Jellinek, A.M., Manga, M., 2004. Links between long-lived hotspots, mantle plumes, D″, and plate tectonics. Rev. Geophys. 42.

Kellogg, L.H., Hager, B.H., van der Hilst, R.D., 1999. Compositional stratification in the deep mantle. Science 283, 1881–1884.

Knittle, E., Jeanloz, R., 1991. The high pressure phase diagram of $FeO_{0.94}$: a possible constituent of the Earth's core. J. Geophys. Res. 96, 16169–16180.

Labrosse, S., Hernlund, J.W., Coltice, N., 2007. A crystallizing dense magma ocean at the base of Earth's mantle. Nature 450, 866–869.

Lay, T., Hernlund, J., Garnero, E.J., Thorne, M.S., 2006. A post-perovskite lens and D″ heat flux beneath the central pacific. Science 314, 1272–1276.

Lithgow-Bertelloni, C., Richards, M.A., 1998. The dynamics of Cenozoic and Mesozoic plate motions. Rev. Geophys. 36, 27–78.

Mao, W.L., Meng, Y., Shen, G., Prakapenka, V.B., Campbell, A.J., Heinz, D.L., Shu, J., Caracast, R., Cohen, R.E., Fei, Y., Hemley, R.J., Mao, H.-K., 2005. Iron-rich silicates in the Earth's D″ layer. Proc. Natl. Acad. Sci. 102, 9751–9753.

Mao, W.L., Mao, H., Sturhahn, W., Zhao, J., Prakapenka, V.B., Meng, Y., Shu, J., Fei, Y., Hemley, R.J., 2006. Iron-rich post-Perovskite and the origin of the ultralow velocity zones. Science 312, 564–565.

Masters, G., Johnson, S., Laske, G., Bolton, H., 1996. A shear-velocity model of the mantle. Philos. Trans. R. Soc. Lond. A 354, 1385–1411.

McNamara, A.K., Zhong, S., 2004. Thermochemical structures within a spherical mantle: superplumes or piles? J. Geophys. Res. 109.

McNamara, A.K., Zhong, S., 2005. Thermochemical structures beneath Africa and the Pacific. Nature 437, 1136–1139.

Mégnin, C., Romanowicz, B., 2000. The shear-wave velocity structure of the mantle from the inversion of body, surface and higher modes waveforms. Geophys. J. Int. 143, 709–728.

Mégnin, C., Bunge, H.P., Romanowicz, B., Richards, M.A., 1997. Imaging 3-D spherical convection models: what can seismic tomography tell us about mantle dynamics? Geophys. Res. Lett. 24, 1299–1302.

Menke, W., 1989. Geophysical Data Analysis: Discrete Inverse Theory. Elsevier, New York. 289 pp.

Montelli, R., Nolet, G., Dahlen, F.A., Masters, G., Engdahl, E.R., Hung, S.-H., 2004. Finite-frequency tomography reveals a variety of plumes in the mantle. Science 303, 338–343.

Murakami, M., Hirose, K., Kawamura, K., Sata, N., Ohishi, Y., 2004. Post-perovskite phase transition in $MgSiO_3$. Science 304, 855–858.

Ni, S., Tan, E., Gurnis, M., Helmberger, D.V., 2002. Sharp sides to the African superplume. Science 296, 1850–1852.

Nolet, G., Karato, S.-I., Montelli, R., 2006. Plume fluxes from seismic tomography. Earth Planet. Sci. Lett. 248, 685–699.

Oganov, A.R., Ono, S., 2004. Theoretical and experimental evidence for a post-perovskite phase of MgSiO3 in Earth's D″ layer. Nature 430, 445–448.

Ohta, K., Hirose, K., Lay, T., Sata, N., Ohishi, Y., 2008. Phase transitions in pyrolite and MORB at lowermost mantle conditions: implications for a MORB-rich pile above the core–mantle boundary. Earth Planet. Sci. Lett. 267, 107–117.

Ricard, Y., Richards, M., Lithgow-Bertelloni, C., 1993. A geodynamic model of mantle density heterogeneity. J. Geophys. Res. 98, 21895–21909.

Richards, M.A., Bunge, H.-P., Lithgow-Bertelloni, C., 2000. Mantle convection and plate motion history: toward general circulation models. In: Richards, M.A., et al. (Ed.), The History and Dynamics of Global Plate Motions. . Geophysical Monograph Series, vol. 121. American Geophysical Union, pp. 289–307.

Ritsema, J., Ni, S., Helmberger, D.V., Crotwell, H.P., 1998. Anomalous shear velocity reductions and gradients in the lower mantle beneath Africa. Geophys. Res. Lett. 25, 4245–4248.

Ritsema, J., van Heijst, H.J., Woodhouse, J.H., 1999. Complex shear-wave velocity structure imaged beneath Africa and Iceland. Science 286, 1925–1928.

Ritsema, J., van Heijst, H.J., Woodhouse, J.H., 2004. Global transition zone tomography. J. Geophys. Res. 109.

Ritsema, J., McNamara, A.K., Bull, A.L., 2007. Tomographic filtering of geodynamic models: implications for model interpretation and large-scale mantle structure. J. Geophys. Res. 112.

Schubert, G., Masters, G., Olsen, P., Tackley, P., 2004. Superplumes or plume clusters? Phys. Earth Planet. Inter. 146, 147–162.

Simmons, N.A., Forte, A.M., Grand, S.P., 2007. Thermochemical structure and dynamics of the African superplume. Geophys. Res. Lett. 34.

Stixrude, L., Lithgow-Bertelloni, C., 2005. Thermodynamics of mantle minerals – I. Physical properties. Geophys. J. Int. 162, 610–632.
Su, W.J., Woodward, R.L., Dziewonski, A.M., 1994. Degree 12 model of shear-wave velocity in the mantle. J. Geophys. Res. 99, 6945–6980.
Tackley, P.J., 1998. Three-dimensional simulations of mantle convection with a thermochemical CMB boundary layer: D″? In: Gurnis, et al. (Ed.), The Core–Mantle Boundary Region. American Geophysical Union, pp. 231–253.
Tackley, P.J., 2002. Strong heterogeneity caused by deep mantle layering. Geochem. Geophys. Geosys. 3.
Tan, E., Gurnis, M., 2005. Metastable superplumes and mantle compressibility. Geophys. Res. Lett. 32.
Tan, E., Gurnis, M., 2007. Compressible thermochemical convection and application to lower mantle structures. J. Geophys. Res. 112.
van der Hilst, R.D., Widiyantoro, S., Engdahl, E.R., 1994. Evidence of deep mantle circulation from global tomography. Nature 386, 578–584.
van der Hilst, R.D., De Hoop, M.V., Wang, S.H., Shim, L., Tenorio, L., Ma, P., 2007. Seismostratigraphy and thermal structure of Earth's core–mantle boundary region. Science 315, 1813–1817.
Wang, Y., Wen, L., 2004. Mapping the geometry and geographic distribution of a very low velocity province at the base of the Earth's mantle. J. Geophys. Res. 109.
Workman, R.K., Hart, S.R., 2005. Major and trace element composition of the depleted MORB mantle (DMM). Earth Planet. Sci. Lett. 231, 53–72.
Zhong, S., Hager, B.H., 2003. Entrainment of a dense layer by thermal plumes. Geophys. J. Int. 154, 666–676.
Zhong, S., Zuber, M.T., Moresi, L., Gurnis, M., 2000. Role of temperature-dependent viscosity and surface plates in spherical shell models of mantle convection. J. Geophys. Res. 105, 11063–11082.